Do ambient shear and thermal stratification impact wind turbine tip-vortex breakdown?

Do ambient shear and thermal stratification impact wind turbine tip-vortex breakdown?

Amy Hodgkin[1], Sylvain Laizet[1], Georgios Deskos[2]

[1]Department of Aeronautics, Imperial College, London SW7 2AZ, UK
[2]National Wind Technology Center, National Renewable Energy Laboratory, Golden, Colorado 80401, USA

E-mail: a.hodgkin19@imperial.ac.uk

Abstract. Modern wind turbines experience uneven inflow conditions across the rotor, due to the ambient flow's shear and thermal stratification. Such conditions alter the shape and length of turbine wakes and thus impact the loads and power generation of downstream turbines. To this end, understanding the spatial evolution of the individual wakes under different atmospheric conditions is key to controlling and optimising turbine arrays. With this numerical study we aim to obtain a better understanding of the fundamental physics governing the near-wake dynamics of wind turbines under shear and thermal stability, by examining their tip-vortex breakup mechanisms. Our approach considers scale-resolving simulations of a single turbine wake under a linear shear profile as well as the application of harmonic tip perturbations to trigger flow instabilities. For the subsequent analysis we use the proper orthogonal decomposition (POD) method to extract coherent structures from the flow, and we also calculate mean kinetic energy fluxes to quantify each coherent structure's contribution to wake recovery. The wake's helical spiral is found to hinder wake recovery for all studied ambient flow conditions, whereas the mutual inductance instability has positive MKE flux leading to an enhanced wake recovery. Finally, the ambient shear has the largest impact on the local MKE flux with respect to downstream location by changing the shape of the curve and location of extrema, whereas thermal stratification has only a minimal impact on the magnitude of the near-wake local MKE flux distribution.

1. Introduction

Modern large–scale offshore wind farms consist of multiple turbines clustered together in turbine arrays to scale up energy production. Such a clustering exhibits several drawbacks during the operation of the wind farm, as some of the downstream turbines will inevitably have to operate within the wake of the upstream ones. A wind turbine operating within a wake field is not ideal for two reasons. First, the apparent reduction of its power output due to the wind speed de-acceleration and second, an increase of the fatigue loads due to experiencing the upstream wake-laden turbulence. Power losses due to wake effects were reported to be in the order of 10–25% while the fatigue-related failures were reported to be around the same levels owing to a limited understanding of the offshore turbulence [1, 2].

Turbine wakes are subject to a complex ambient environment which is characterised by strong shear, veer, thermal stratification and terrain specific large-coherent structures [3]. In particular, thermal stratification is a key parameter of atmospheric boundary layer (ABL) as it impacts the mean velocity profile (shear), as well as the intensity and structure of turbulence. Thermal

stratification is also used to classify the atmospheric surface layer into a neutral, unstable (convective) and stable ABL. The combination of shear and positive thermal stability can have a profound effect on wind turbines wake's properties. In quantifying the wake characteristics (length, expansion etc) under shear and thermal stratification, it is important to be able to identify a stable wake length which is defined as the length of the wake region extending from the rotor plane, where helical vortex structures are shed from the blades' tips, to the location where the tip-vortex system breaks down to turbulence. As tip-vortices break up into smaller structures, the near-wake field transitions to a far-wake field which consists of smaller turbulent structures that are rapidly mixing with the ambient fluid [4]. The magnitude of the stable wake length can be impacted by multiple factors including, thermal stratification and the mean shear profile. Early work by Widnall [5] identifies the mutual inductance instability as one of three main instabilities leading to vortex breakdown. It arises when neighbouring tip-vortex filaments are disturbed with out-of-phase perturbations, causing vortex pairing to occur.

In this work, the break-up mechanisms of wind turbine tip-vortices within ambient flow with shear and thermal stratification are investigated using high-fidelity, turbulence-resolving simulations. Our model serves as a simplified version of the turbulent conditions experienced by utility-scale wind turbines, and aims at extracting information relevant to the stability mechanisms inherent to the helical, tip-vortex system. Previous works look only at the influence of moderate shear, with no thermal stratification. Our focus is on the near-wake field (few diameters downstream of the wind turbines). The influence of the mutual inductance instability [5] on the breakdown under various shear and thermal stratification intensities is studied by imposing a single harmonic perturbation near the tip blades which triggers flow instabilities and allows the wake's transition to turbulence. This idealised set-up allows us to better understand the influence of each parameter, with a focus on the combined effects of shear, thermal stratification and the frequency of the harmonic perturbation.

2. Methodology

Turbulence-resolving simulations of a single three-bladed scale turbine are carried out using the wind farm simulator `WInc3D` [6] which is part of the open-source framework of flow solvers `XCompact3D` [7].The simulations are based on the incompressible Navier-Stokes and temperature scalar transport equations, coupled through a gravitational term. These equations are solved with sixth-order finite-difference schemes on a Cartesian mesh while a conventional actuator line method is used to model the turbine via a forcing term added to the momentum equation. More details about the numerical methods implemented in `WInc3D` can be found in Laizet et al. [8, 9]. For this study a positive vertical velocity gradient and temperature gradient are imposed to study the effects of shear and thermal stratification on the wake. The incompressible Navier-Stokes and potential temperature advection equations can be expressed as,

$$\frac{\partial u_i}{\partial x_i} = 0, \tag{1}$$

$$\frac{\partial u_i}{\partial t} = -\frac{1}{2}\left(u_j\frac{\partial u_i}{\partial x_j} + \frac{\partial u_i u_j}{\partial x_j}\right) - \frac{\partial p}{\partial x_i} + \frac{1}{Re}\mathcal{D} + F_i, \tag{2}$$

$$\frac{\partial \theta}{\partial t} = -u_j\frac{\partial \theta}{\partial x_j} + \frac{1}{Re\cdot Sc}\mathcal{Q}, \tag{3}$$

where u_i is the velocity vector field, p the pressure field, θ is the potential temperature and F_i accounts for additional forcing, including the buoyancy force. $i = 1, 2, 3$ corresponds to the streamwise (x), vertical (y) and spanwise (z) directions, respectively. $Re = U_0 R/\nu$ is the Reynolds number, where U_0 is the reference velocity, R is the turbine radius, and ν is the kinematic viscosity, and Sc is the Schmidt number. The implicit large-eddy simulation (iLES)

approach of Dairay et al. [10] is used to handle the subgrid scales through a momentum diffusion term, $\mathcal{D}$, and temperature diffusion term, $\mathcal{Q}$. The present iLES approach is based on a strategy that introduces targeted numerical dissipation at the smaller scales through the discretisation of the second derivatives of the viscous terms and has been tested extensively for wind turbines flows [11].

The three-bladed turbine of radius R is a scale-model of the turbine used in NTNU's wind tunnel experiments [12]. The turbine rotor is placed in the mid-height of our computational domain with size $10R \times 10R \times 10R$ and at $2R$ downstream the entrance. The streamwise location of the turbine is referred to as $x = 0$. The mesh is uniform in the three spatial directions with $513 \times 513 \times 513$ mesh nodes. The Reynolds number is $Re = 30,000$ and the tip speed ratio is $\lambda = \Omega R/U_0 = 6$, where Ω is the angular velocity of the turbine.

The influence of shear on the wake is investigated by imposing a uniform vertical velocity gradient at the inflow, which is maintained with free-slip boundaries in the vertical and spanwise directions. The influence of thermal stratification is investigated by imposing a uniform vertical temperature gradient throughout the domain. This is maintained with fixed-temperature boundary conditions in the vertical directions, equal to the initial values at these locations. We define the strengths of these two properties as a percentage change, from the reference value (at the centre of the turbine), across a rotor turbine radius.

Harmonic tip perturbations are added around the blade tips to trigger instabilities and allow tip-vortices to breakdown into turbulence , without this added disturbance the tip-vortices would theoretically continue forever. A single frequency perturbation allows the vortex structure and influence of the mutual inductance instability to be be clearly observed. This is done with a force term in the Navier-Stokes equations applied in the streamwise direction:

$$F_p = A \sin(k_p \Omega t), \tag{4}$$

where k_p is the wavenumber and the amplitude of the perturbation, A, is selected so that it gives a maximum turbulence intensity of 0.5% assuming a uniform ambient flow. The perturbation is applied in a region of $0.5R$ on either side of the blade in the streamwise direction and from $0.75R$ to $1.25R$ in the radial direction. Once the flow has become fully established, 600 snapshots of the flow field are saved every 0.05 s and subsequently used for our analysis.

The discretisation of the blades within the actuator line method uses 100 blade elements and a look-up table specific to the turbine's airfoil characteristics evaluates the lift, drag and pitch moment coefficients all based on the local Reynolds number. Additionally, a tip loss correction factor [13] is used near the tip of the blade. For the velocity boundary conditions, we consider a free-slip in the vertical and spanwise directions and inflow/outflow boundary conditions in the streamwise direction with a uniform inflow velocity field applied at the inlet and a 1D convection equation at the outlet to effectively advect the turbulent wake outside of our computational domain. The time step for the present simulation is 0.0005 s which guarantees a CFL number less than 0.1.

The main data analysis presented in this paper is based on proper orthogonal decomposition (POD) which extracts the coherent structures of the flow [14] based on their energy content. The decomposition method finds a set of orthogonal basis vectors from which the complete velocity field can be reconstructed.

$$u_i = \overline{u}_i + \sum_{k=1}^{N} \phi_i^k a_k, \tag{5}$$

where $\bar{\cdot}$ indicates the averaged quantity over all snapshots, index k corresponds to the k^{th} mode velocity field, in descending order of their energy contribution to the flow, ϕ_i^k is the velocity of mode k in direction i, and a_k is the corresponding temporal coefficient (amplitude).

The mean kinetic energy (MKE) flux, of the POD modes is computed to gain insight into how each energy mode impacts the wake breakdown [15]. The approximation,

$$\overline{u_i' u_j'} \approx \overline{\sum_{k=1}^{N}(a_k \phi_i^k) \sum_{l=1}^{N}(a_l \phi_i^l)} = \sum_{k=1}^{N}\sum_{l=1}^{N} \overline{a_k a_l}\phi_i^k \phi_j^l = \sum_{k=1}^{N} \lambda_k \phi_i^k \phi_j^k, \tag{6}$$

where λ_k is the eigenvalue of mode k, is used to relate the turbulent MKE term, $-\frac{\partial}{\partial x_j}\left(\overline{u}_i \overline{u_i' u_j'}\right)$, which is extracted from the MKE transport equation, to a single POD mode. The local MKE flux, which is a function of x, is found by integrating the turbulent MKE term across 2D slices in the y-z plane which encircle the wake. We use a circular control area, A_c, with radius $R_c = 1.2R$ in this work. The local MKE flux is then normalised by the circumference of the enclosed area:

$$f_T^k(x) = \frac{1}{2\pi R_c} \int_{A_c} -\frac{\partial}{\partial x_j}\left(\overline{u}_i \lambda_k \phi_i^k \phi_j^k\right) dydz \tag{7}$$

The complete study is made up of 27 simulations, consisting of 3 perturbation frequencies ($k_p = 0$, 3/2 and 9/2), 3 shear strengths (0, 10% and 20%) and 3 thermal stratification strengths (0, 1% and 2%), corresponding to values observed in real wind farms. This present manuscript only presents a selection of results, mainly focusing on the perturbed cases ($k_p = 3/2$ and 9/2). Note finally that the simulations without thermal stratification have been successfully validated with the data of Kleusberg et al. [16] (data not presented here for conciseness, see Hodgkin et al. [17] for more details).

The focus of this study is not to represent operational conditions with a fully turbulent flow (this is also why we do not simulate the boundary layer). Instead, we investigate the influence of shear, thermal stratification and tip perturbations in an idealised set-up and focus on the mechanisms inherent to the helical tip-vortex system which once triggered lead to destabilisation and transition to turbulence. A stability study in a fully turbulent atmospheric boundary layer would not be able to shed light into the mechanisms, as it would not be possible to distinguish between the impact of different factors such as shear, thermal stratification, veer and wall effects.

3. Results

3.1. Wake Shape and Vorticity

We start the presentation of our results by describing the effect of shear and thermal stratification on the wake shape and vorticity fields. First, shear is found to impact the development of the wake by lengthening the wake along the top and shortening it along the bottom. The vorticity contours from $x = 0$ to $4R$, in Figure 1, show the wake as it expands downstream of the turbine for cases with no thermal stratification. It has been shown in Hodgkin et al. [17] that thermal stratification has only a minor impact on the wake footprint with no effect on the breakdown to turbulence location. Without perturbation ($k_p = 0$), nor shear, the wake can be characterised by a helical spiral that gradually expands radially as it evolves downstream of the turbines, without breaking down to turbulence in the computational domain of interest. The selected non-zero wavenumbers correspond to out-of-phase perturbations, triggering neighbouring vortex lines to interact with each other (mutual inductance instability). As can be seen in Figure 1, the wake breaks down when neighbouring vortex lines interact, which happens sooner for the $k_p = 3/2$ cases. A consequence of shear is that the helical vortices are convected faster at the top than at the bottom, as clearly seen in cases where a zero perturbation is applied. As a result, the spacing between vortex lines, also called the streamwise vortex separation distance, is larger at the top compared to the bottom, resulting in vortex pairing occurring first at the bottom.

Looking closer at the streamwise evolution of the near wake, it is possible to define three distinct regions in the wake, based on the shape of the vortex lines: linear, transition and

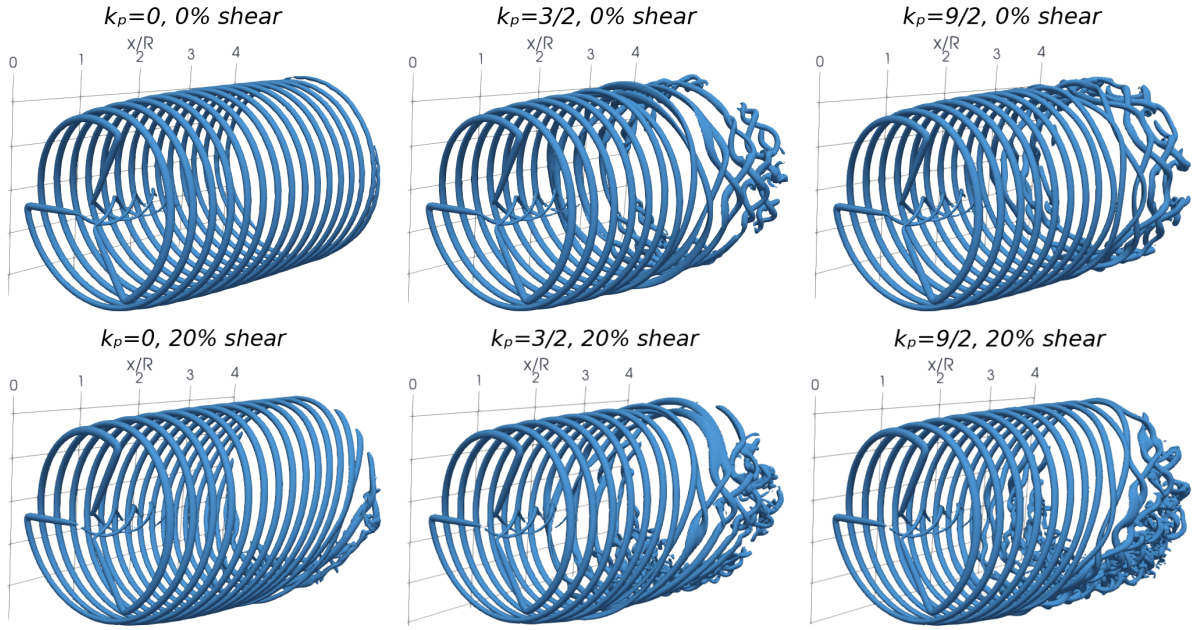

Figure 1. Vorticity contours for 6 selected cases with no thermal stratification, spanning from $x = 0$ to $x = 4R$.

turbulent. The linear region extends from $x = 0.5R$ (to ignore hub effects) until the vortex lines show the first signs of disturbance. For $k_p = 3/2$ this region ends at $x = 1.5R$ and for $k_p = 9/2$ at $x = 1.8R$. Next, the transition region extends until neighbouring vortex lines first overlap, which can be placed at $x = 2R$ for $k_p = 3/2$ and $x = 2.8R$ for $k_p = 9/2$. Finally, the turbulent region starts at end of the transition region and extends onward.

3.2. Thrust and Power

For context, we looked briefly at the average thrust and power output differences for each inflow. The average is taken over a set of snapshots taken every second. The maximum thrust is found for the uniform inflow for each perturbation frequency. The least thrust is found for the 20% shear + 1% thermal stratification case and is approximately 2% less than the thrust at uniform. The maximum average power is achieved for the 20% shear cases, and is about 0.8% larger than the power for uniform inflow. The 20% shear + 1% thermal stratification cases produce the least power; roughly 3% less than the power for uniform inflow for all cases.

3.3. Proper Orthogonal Decomposition and Coherent Structures

A POD analysis is carried out on the wake from 0 to $4R$ downstream of the blades, in order to focus only on the near-field flow dynamics. Note that the root vortex is removed before the post-processing of the data. The POD modes can be presented in pairs, each with the same structure but with a phase shift. In the present study, the focus is on the two most dominant POD mode pairs, as they are very energetic and drive the flow. For each perturbation one pair of modes has a helical shape and seems to relate to the helical spiral vortex. The other mode shape sees distinct 'lobes' which correlate to half a wavelength of the perturbation, hence is related to the mutual inductance instability. For $k_p = 9/2$ there are nine lobes, and only three lobes for $k_p = 3/2$. For simplicity these mode shapes are labelled the helical spiral pair and the mutual inductance pair, respectively, as they relate to these phenomena. The order of dominance of the pairs depends on the perturbation frequency. 2D slices of these modes at the centre of each

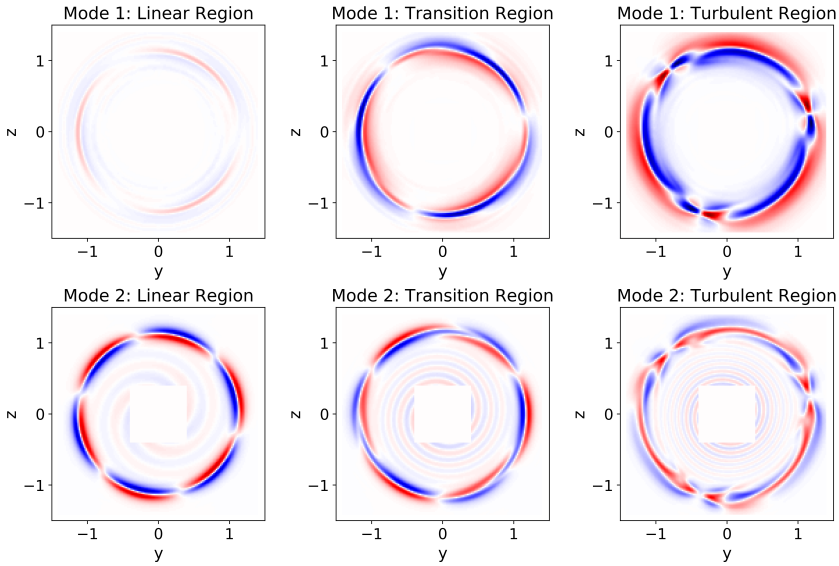

Figure 2. 2D y-z planes of the two most dominant mode pairs, plotted in the centre of the linear ($x = 1R$), transition ($x = 1.75R$) and turbulent ($x = 2.5R$) regions for $k_p = 3/2$ without shear or thermal stratification. Red colour shows a positive isocontour and blue colour shows a negative isocontour.

defined local region (linear, transition and turbulent) are shown in Figure 2 and Figure 3 for the uniform case of each perturbation (no shear and no thermal stratification). The uniform flow allows the shape of the mode to be clearly observed. The shape of the modes stays roughly the same as they are convected downstream from the blades but the strength of the mode (shown by the strength of the colour) changes and the shape is eventually impacted by the vortex pairing and the transition to turbulence. $k_p = 9/2$ is higher frequency than $k_p = 3/2$, hence triggering a wider range of small turbulent scales (with only three lobes for $k_p = 3/2$ and nine lobes for $k_p = 9/2$). When shear and thermal stratification are present (not shown here for conciseness), the general structure of modes stays the same, but shear causes the helical spiral mode lines to slant, and the mutual inductance to grow in magnitude sooner at the bottom of the wake. The area of the mode shapes both change in line with the wake area. Thermal stratification has only a limited impact on the shape of the dominant pair of POD modes.

The flow complexity can be inferred from the percentage energy in a finite selection of POD modes. Figure 4 shows the energy percentage contained in the first ten pairs of modes. An exponential decay can be seen for pairs of modes 3 to 10, with a minimum regression coefficient of -0.9 for all cases. Similar trends were reported in Nemes el at. [18] in an experimental investigation of the mutual inductance instability. For $k_p = 3/2$ with 20% shear and 1% or 2% thermal stratification the exponential fit is the closest (≤ -0.99). With the same amount of shear but no thermal stratification, the fit is reduced (-0.9). For $k_p = 9/2$ all cases with thermal stratification have a close exponential fit (≤ -0.975), and those without thermal effects are slightly less (≥ -0.96). The cases with no shear and 10% shear have the quickest decay, while all the other setups decay at a similar rate, indicating that they are of similar flow complexity. The case with 20% shear and 1% thermal stratification has the shallowest decay for the first 10 pairs of modes, potentially indicating the most complex flow (in terms of structures) as less energetic modes still have a certain amount of energy, with an impact on the development of the wake. Interestingly, the shear and thermal stratification strength of this idealised setup are similar to values found in the stable atmospheric boundary layer set up of Abkar and Porté-Agel

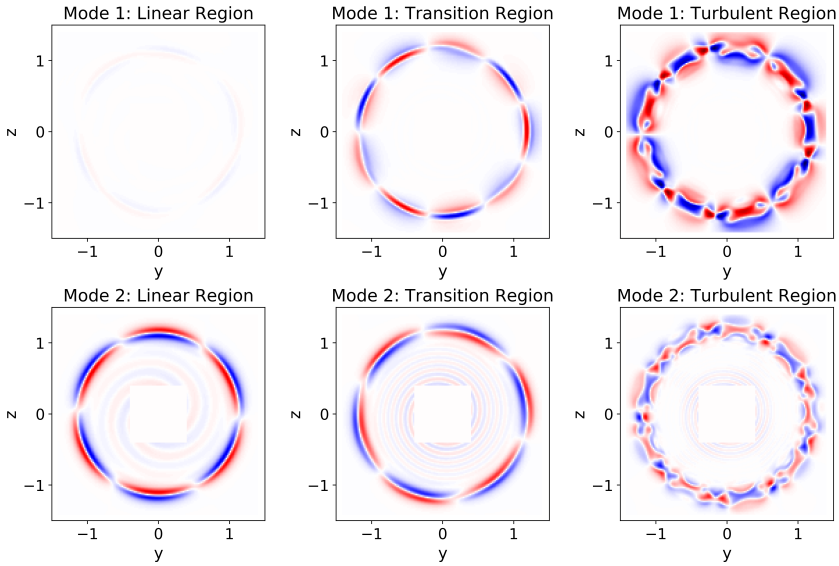

Figure 3. 2D y-z planes of the two most dominant mode pairs, plotted in the centre of the linear ($x = 1.15R$), transition ($x = 2.3$) and turbulent ($x = 3.3$) regions for $k_p = 9/2$ without shear or thermal stratification. Red colour shows a positive isocontour and blue colour shows a negative isocontour.

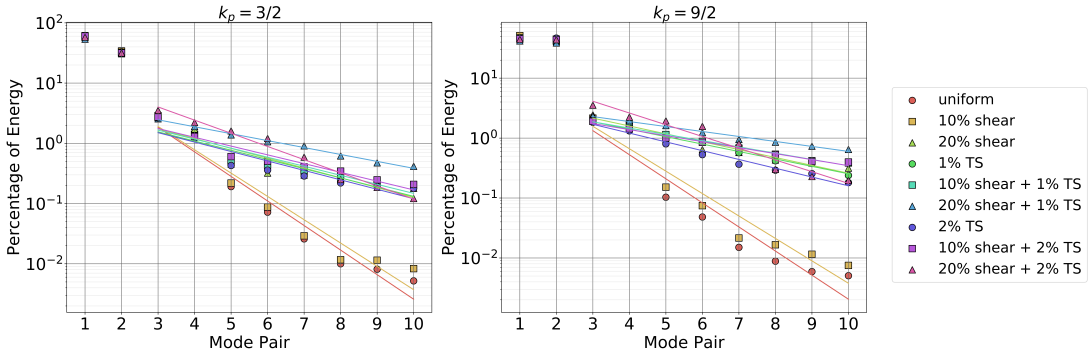

Figure 4. Percentage energy contained in the first ten pairs of POD modes from $x = 0.5R$ to $x = 3.5R$ with a line of best fit plotted to show a potential exponential decay from pairs of modes three to ten. TS means thermal stratification.

[19]. As a comparison, Ali et al. [20] found that to capture 50% of the turbulent kinetic energy, the stable boundary layer requires 200% more modes than the unstable boundary layer.

3.4. Mean Kinetic Energy and Wake Recovery

To further understand the impact of the coherent structures on the wake breakdown, the MKE flux for each mode can be used. A positive MKE flux indicates that turbulent energy is being transferred from the ambient fluid to the wake, hence it accelerating wake breakdown. Conversely, a negative MKE flux suggests the structure is inhibiting wake breakdown. Plots of the local MKE flux are shown in Figure 5 and Figure 6 for the helical spiral and mutual inductance pairs of modes only, as they are the most dominant ones. The control area, of $1.2R$ radius, is selected as it encloses completely the wake downstream of the blades up to at least $1R$ for all cases. The radius of the control area is arbitrary and is not perfect as the wake

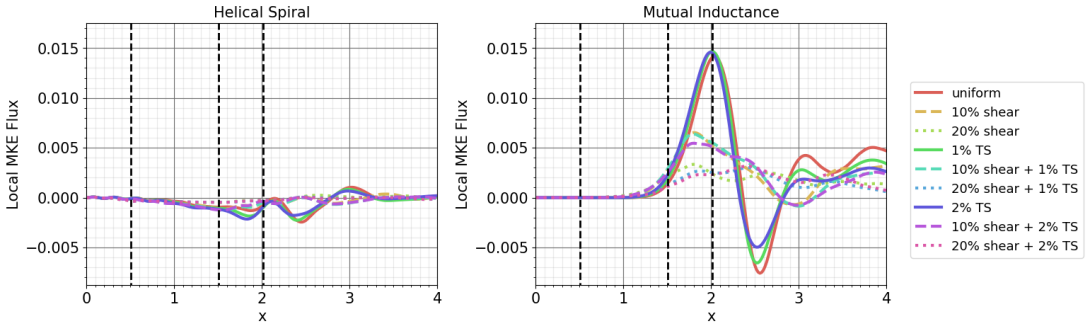

Figure 5. $k_p = 3/2$: Local MKE flux as a function of the streamwise distance from the blades for the two dominant pairs of modes for a circular control area with a radius of 1.2R.

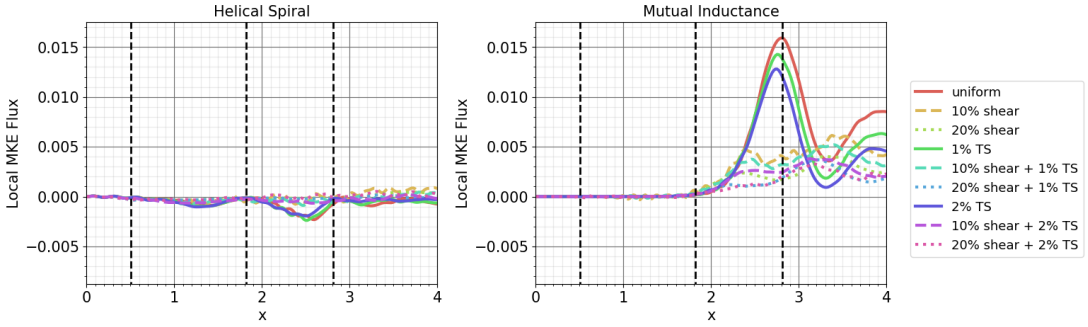

Figure 6. $k_p = 9/2$: Local MKE flux as a function of the streamwise distance from the blades for the two dominant pairs of modes for a circular control area with a radius of 1.2R.

expands differently for each case, however it is big enough to enclose the main features of the wakes. The local MKE flux shows how each coherent structure is impacting the recovery of the wake as a function of the streamwise distance from the blades. The helical spiral pair of modes has a predominantly negative local MKE flux, with some small positive values, notably between $x = 2.8R$ and $x = 3.2R$ for $k_p = 3/2$ and in the turbulent region for $k_p = 9/2$. The helical spiral's total MKE flux, which is integrated through the region in x, for each defined region is always negative. This confirms previous published results suggesting that the helical spiral delays the breakdown to turbulence [21, 15] and will not breakup without additional disturbance. The mutual inductance instability gives the positive MKE flux needed to disrupt the wake and break up the tip-vortices. The mutual inductance pair of modes has a positive local MKE flux, apart from for $k_p = 3/2$ no shear cases where flux is negative between $x = 2.3R$ and $x = 2.8R$. The total MKE flux for the mutual inductance is positive in each region, therefore contributing to the breakdown of turbulence. The dotted vertical lines on the figures correspond to the start of the linear, transition and turbulent regions which are defined based on the vortex line interactions.

The local MKE flux of the mutual inductance pair is shown on the right of Figure 5 for $k_p = 3/2$. With low shear, the flux oscillates from positive to negative. For all cases, there is no flux until about $x = 1.4R$ where the flux increases. The transition region begins at the start of this growth period. When there is no shear present the MKE flux grows steeply until it reaches a maximum at $x = 2R$. This is the start of the turbulent region. At $x = 2R$ the radius of the vortex is approx $1.2R$, which correlates with the maximum value being found at this location (after this streamwise location, the vortex lines are outside of the control volume). Thermal stratification has little impact on the location of the maximum value for the flux. After reaching

a maximum value, the flux then decreases until it becomes negative at $x = 2.3R$, and a global minimum is found at about $x = 2.5R$. The mutual inductance pair of modes is not contributing to the wake recovery when negative, but the vortex is outside the $1.2R$ radius here which could explain why a negative value is found. When thermal stratification is present the minimum value is slightly smaller in magnitude. When shear is present the shape of the curve flattens out, and the large global extrema are reduced and local turning points appear. This could be explained by the two streamwise locations for the breakdown (top and bottom of the wake as the vortex lines are slanted) and there is a trade off between the bottom being turbulent earlier than the top. With 10% shear, there is a global maximum at $x = 1.8R$, followed by a small reduction and then a local maximum at $x = 2.4R$. The location of the maxima roughly correlate with the bottom becoming turbulent at $x = 1.8R$ and the top becoming turbulent around $x = 2.3R$. At $x = 1.8R$ the radius at the top is $1.13R$, and at the bottom it is $1.24R$ while at the sides it is around $1.2R$. At $x = 2.4R$, the radius at the top is $1.15R$, $1.27R$ at the bottom and $1.2R$ at the sides. There is a minimum at $x = 3R$ which is a negative value. The 20% shear cases give rise to the flattest curve where it is hardest to pick out maxima and minima. There are maxima at around $x = 1.8R$ and $x = 2.4R$ which are at the same locations as for the cases with 10% shear. The magnitude of these maxima is smaller than for the 10% shear cases. With no thermal stratification, the curve is slightly different from the cases with thermal stratification. For this shear strength, the bottom is turbulent from around $x = 1.6$ and the top is laminar until about $x = 3R$. Therefore the maxima locations do not seem to be related to the start of the transition regions. This could be explained by the big difference for the radius of the wake at the top and bottom when shear is present, which is influencing the flux more than the streamwise location of the transition region.

Figure 6 shows the streamwise evolution of the flux for the cases with $k_p = 9/2$. The local MKE flux for the mutual inductance pair of modes is always positive, unlike the $k_p = 3/2$ cases which have a large negative minimum for the cases with no shear. For all cases in this figure, the flux starts to grow at approximately $x = 1.8R$, which is where the transition begins and the vortex lines first begin to oscillate and become curved. When there is no shear, there is one maximum at $x = 2.8R$, very close to the start of the turbulent region. Note that at this location, the vortex lines are just outside the 1.2R control volume radius. Thermal stratification reduces the magnitude of the flux and shifts the extrema slightly downstream of the blades. There is a minimum at $x = 3.3R$, but with positive values. The shear flattens the curve shape, with no obvious local minimum. For the cases with 10% shear, there is a maximum at $x = 2.4R$ and again around $x = 3.3R$, which roughly correlate with breakdown locations at the top and bottom of the wake. The second maximum is larger than the first, as is the case with $k_p = 3/2$. Thermal stratification reduces the magnitude of the maximum values. The flattest curve is observed for the 20% shear cases, but with a similar streamwise location for the maximum values to the 10% shear cases. The addition of thermal stratification only slightly changes the flux values.

The cases for the two studied perturbation frequencies have similar trends up to the beginning of the turbulent region for the mutual inductance pair of modes. The local MKE flux grows until it reaches a maximum at the beginning of the defined turbulent region. This period of growth is steeper for $k_p = 3/2$ than for $k_p = 9/2$ and it correlates with a shorter transition period for these cases. The other key difference is that the $k_p = 3/2$ cases, especially with no shear and large extrema values, have a period in which there is negative local flux, unlike the $k_p = 9/2$ cases which always remain positive. This trend will have to be investigated further but might be related to the size of the control area.

4. Conclusions

In this numerical study, 27 high-fidelity simulations of a turbine wake were generated using the actuator line method to assess the effect of shear and thermal stratification on the near-wake

field vortex dynamics. To trigger the breakup of the tip-vortices into turbulence, a perturbation with different wavelengths was applied at the blade tips to promote the mutual inductance instability.

The results show that the impact of shear on the wake shape and perturbation growth is large whereas thermal stratification has only a limited impact on the near-wake footprint. The signature of the perturbation can clearly be seen with the most dominant POD modes. Most of the energy of the wake is recovered with only two pairs of POD modes, corresponding to the helical spiral pair and the mutual inductance pair. The eigenvalues of mode pairs 3-10 fit a decaying exponential trend, with the uniform case having the steepest decay and 20% shear + 1% thermal stratification having the shallowest decay. The two dominant pairs of modes drive the flow and the breakdown to turbulence. Analysis of the MKE flux for these pairs indicate that shear and thermal stratification reduce the influence of the perturbation and the shielding effect of the helical spiral. Moreover, the local MKE flux of the helical spiral is small in magnitude and almost always negative, whereas the local MKE flux of the mutual inductance pair has larger variations in magnitude and is impacted by shear and thermal stratification. When there is no shear the maximum of local MKE flux for the mutual inductance pair is found at the beginning of the turbulent region, which is defined as the location where neighbouring vortex lines have crossed. The shape of the local MKE flux curve is changed by the shear intensity, with two maxima observed near the transition points at the top and bottom for 10% shear. 20% shear leads to an even flatter curve, and maxima do not line up with the transition locations. The streamwise location of maxima and minima depend mostly on the shear intensity. Finally, our analysis indicates that thermal stratification has a lesser impact on the local MKE flux, as it may alter the magnitude of the curve, but not to the extent of causing a significant change to the shape of the curve. Future work will use similar analysis methods while expanding the parameter space to investigate impact of veer, unstable boundary layer and control methods to shorten the stable wake.

5. Acknowledgements

The authors thank EPSRC for the computational time made available on the UK supercomputing facility ARCHER via the UK Turbulence Consortium (EP/R029326/1 and EP/V000942/1). Computational time was also provided by PRACE via the Irene-Rome supercomputer facilities (grant number: 2019215138). The authors would like to acknowledge the Department of Aeronautics, Imperial College London for supporting this work funded by a PhD studentship.

References

[1] Barthelmie R J, Pryor S C, Frandsen S T, Hansen K S, Schepers J G, Rados K, Schlez W, Neubert A, Jensen L E and Neckelmann S 2010 *Journal of Atmospheric and Oceanic Technology* **27** 1302–1317

[2] Hansen K S, Barthelmie R J, Jensen L E and Sommer A 2012 *Wind Energy* **15** 183–196

[3] Richard J A M S and Charles M 2017 *Annual Review of Fluid Mechanics* **49** 311–339

[4] Vermeer L, Sørensen J N and Crespo A 2003 *Progress in aerospace sciences* **39** 467–510

[5] Widnall S E 1972 *Journal of Fluid Mechanics* **54** 641–663

[6] Deskos G, Laizet S and Palacios R 2020 *Wind Energy* **23** 779–794

[7] Bartholomew P, Deskos G, Frantz R A S, Schuch F N, Lamballais E and Laizet S 2020 *SoftwareX* **12** 100550

[8] Laizet S and Lamballais E 2009 *Journal of Computational Physics* **228** 5989–6015

[9] Laizet S and Li N 2011 *International Journal for Numerical Methods in Fluids* **67**(11) 1735–1757

[10] Dairay T, Lamballais E, Laizet S and Vassilicos J C 2017 *Journal of Computational Physics* **337** 252–274

[11] Deskos G, Laizet S and Piggott M D 2019 *Renewable energy* **134** 989–1002

[12] Krogstad P and Eriksen P E 2013 *Renewable energy* **50** 325–333

[13] Shen W Z, Mikkelsen R, Sørensen J N and Bak C 2005 *Wind Energy* **8** 457–475

[14] Sarmast S, Dadfar R, Mikkelsen R F, Schlatter P, Ivanell S, Sørensen J N and Henningson D S 2014 *Journal of Fluid Mechanics* **755** 705–731

[15] De Cillis G, Cherubini S, Semeraro O, Leonardi S and De Palma P 2021 *Wind Energy* **24** 609–633

[16] Kleusberg E, Benard S and Henningson D S 2019 *Wind Energy* **22** 1789–1799

[17] Hodgkin A, Laizet S and Deskos G 2022 *Wind Energy* In Press

[18] Nemes A, Sherry M, Jacono D L, Blackburn H M and Sheridan J 2014 *Journal of Physics: Conference Series* vol 555 (IOP Publishing) p 012077

[19] Abkar M and Porté-Agel F 2015 *Physics of fluids* **27** 035104

[20] Ali N, Cortina G, Hamilton N, Calaf M and Cal R B 2017 *Journal of Fluid Mechanics* **828** 175

[21] Lignarolo L E M, Ragni D, Scarano F, Ferreira C J S and Van Bussel G J W 2015 *Journal of Fluid Mechanics* **781** 467–493